University of Massachusetts Amherst

July 16, 2010

Draping Films: A Wrinkle to Fold Transition

Alfred Crosby, *University of Massachusetts - Amherst*
D. P. Holmes

Draping Films: A Wrinkle to Fold Transition

Douglas P. Holmes and Alfred J. Crosby

Department of Polymer Science & Engineering, University of Massachusetts, Amherst, Massachusetts, USA[*]
(Received 2 March 2010; published 14 July 2010)

A polymer film draping over a point of contact will wrinkle due to the strain imposed by the underlying substrate. The wrinkle wavelength is dictated by a balance of material properties and geometry; most directly the thickness of the draping film. At a critical strain, the stress in the film will localize, causing hundreds of wrinkles to collapse into several discrete folds. In this Letter, we examine the deformation of an axisymmetric sheet and quantify the force required to generate a fold. We observe that the energy of formation for a single fold scales nearly linearly with the film thickness. The onset of folding, in terms of a critical force or displacement, scales as the thickness to the four-ninth power, which we predict from the energy balance of the system. The folds increase the tension in the remainder of the film causing the radial stress to increase, thereby decreasing the wavelength of the remaining wrinkles.

The wrinkling of soft films commonly exhibits itself everyday in examples ranging from draping fabrics to wrinkled skin. This phenomenon occurs because elastic films bend more easily than they stretch, allowing them to buckle out of plane into wrinkles under applied strain [1]. While wrinkles are smooth undulations that distribute strain evenly, folds are sharp strain localizations of applied strain. Superficially, a wrinkle and a fold appear very similar, but their differences have a profound impact on properties of the deformed media. For a crumpled sheet of paper, a network of folds, not wrinkles, develops and focuses energy in a manner that significantly increases the stiffness of the deformed material [2]. In biological systems, the process of folding is critical to morphogenesis, defining such features as the neural folds in early embryonic development [3]. Wrinkling and folding have garnered much interest recently in patterning [4–6], functional materials [7,8], developable cone dynamics [9], draping [10], crumpling [11–13], and snapping [14,15], yet a fundamental understanding of the relation between the two structures is lacking.

Recently, Pocivavsek and Cerda [16] demonstrated the transition from wrinkling to folding under simple uniaxial compression. Under different geometries, the stresses within the film cannot be neglected as they will in turn cause variations in the film's elastic response. In this Letter, we examine the wrinkle-to-fold transition of a sheet under axisymmetric conditions, which are commonly found in nature (e.g., ciliary body of the eye [3]). We demonstrate that while folds localize strain and lead to a global minimization of energy, the axisymmetry introduces dramatic variations in the stress field of the film thereby impacting the general morphology of the material. These large morphological differences will have an important significance in understanding the growth of soft tissues [17]. In addition, we quantify this transition in terms of both force and displacement; thereby, measuring the energy of fold for-

mation by the simple act of lifting an elastic sheet from the surface of water [Figs. 1(a) and 1(b)].

When a strain, ε, is applied to a thin elastic sheet of thickness h with a Young's modulus E and Poisson's ratio ν, the sheet remains flat while the strain is less than a critical strain, ε_c, where multiple equilibrium states are possible. An increase in strain above ε_c causes the sheet to buckle and bend out of plane into an energetically favorable wrinkled geometry. Cerda and Mahadevan [1] showed that by minimizing the total elastic energy, the wrinkle wavelength and amplitude scale as $\lambda \sim (D/K)^{1/4}$ and $A \sim \lambda \varepsilon^{1/2}$, respectively, where K represents the resistance to
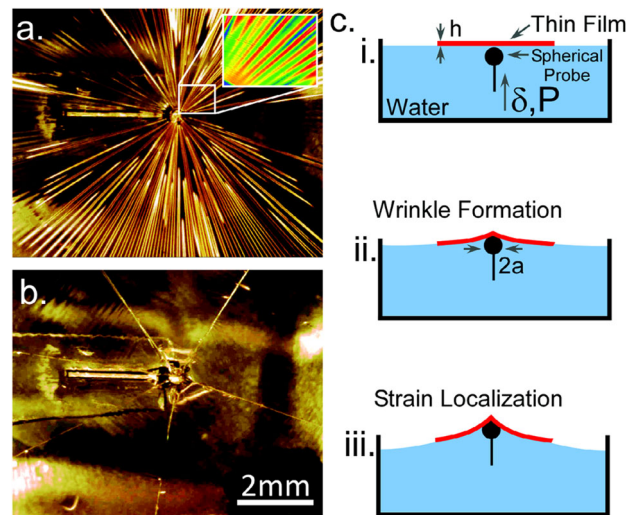

FIG. 1 (color online). (a) Wrinkles on a thin film floating on water lifted by a spherical probe (inset: image via optical profilometry). (b) As the vertical displacement of the probe increases the wrinkles localize into sharp folds. (c) Schematic of the experimental setup, where (i) depicts the axisymmetric thin film floating on water; (ii) the formation of wrinkles as the probe displaces the film vertically, and (iii) the critical displacement at which wrinkles collapse into folds.

stretching, $D = \bar{E}h^3/12$, and $\bar{E} = E/(1 - \nu^2)$ [1,16]. Further strain confining the thin sheet causes the amplitude of wrinkles to increase, concentrating the elastic energy in the strongly bent regions [2]. As the strain increases and amplitude grows, a transition occurs to lower the global energy through strain localization, or folding. These transformations, specifically the nonlinear deformations of thin axisymmetric films, are the focus of this Letter.

For our experiments, a thin polymer film, either poly-dimethylsiloxane (PDMS) (Sylgard 184^{TM}) or polystyrene (PS) (Aldrich), is prepared via spin-coating a polymer solution onto a clean silicon wafer. A circular film of radius $L = 17.5$ mm is floated off the wafer onto the surface of water. A nanopositioner is used to lift a spherical probe of radius $a = 500$ μm by a displacement δ into contact with the center of the film, while a load cell records the force, P, required to deform the film [Fig. 1(c)].

In this geometry, a biaxial stress develops in the thin film upon lifting. To determine the relationship between the centrally applied force, P, and the deflection of the floating film of radius L, we assume that the foundation, i.e., water, will conform to the deflection of the film and will follow the general form of a symmetrically bent circular plate at small displacement away from the plate's edge [18]: $\nabla^4 \delta_r = 0$. Therefore, the deflection is described by $\delta_r = \alpha + \beta r^2 + (P/8\pi D)r^2 \log r$, where the last term accounts for the stress distribution around the single load [18]. Since the radius of the plate is finite, we describe the total strain energy in the system as the summation of the bent plate energy and the energy of deformation for the foundation, which is proportional to the effective elastic stiffness, ρg, where ρ is the fluid density and g is the acceleration due to gravity [19]. The total strain energy is minimized for stable equilibrium, therefore we can determine the general constants, $\alpha = 8P/\pi kL^2$ and $\beta = P/4\pi D$, that provide the relationship between P and the displacement at the center of the film, δ, where $k = \rho g$ [20]. Furthermore, the stress distribution can be determined from the moments or shear force distribution, determined from the plate deflection profile such that

$$\sigma_{rr}^w \sim \rho g \delta \left(\frac{L}{h}\right)^2. \tag{1}$$

By adapting the scaling predictions from Cerda and Mahadevan [1] to a radial geometry [21–23], the number of wrinkles, N, is given by

$$N \sim \left(\frac{\sigma_{rr} a^2}{\bar{E}h^2}\right)^{1/4} \sim C_\delta \bar{E}^{-1/4}h^{-1}, \tag{2}$$

where C_δ is a prefactor defined by $(\rho g \delta L^2 a^2)^{1/4}$. The number of wrinkles for PS and PDMS films with thicknesses ranging from $h = 50$ nm to $h = 13.6$ μm was measured. A plot of N vs $C_\delta \bar{E}^{-1/4}h^{-1}$ from Eq. (2) is given in Fig. 2, and is in very good agreement with Eq. (2). The dashed line represents a slope of unity [24].

Similarly, N is weakly dependent on displacement as shown in a representative plot in Fig. 3, until a critical
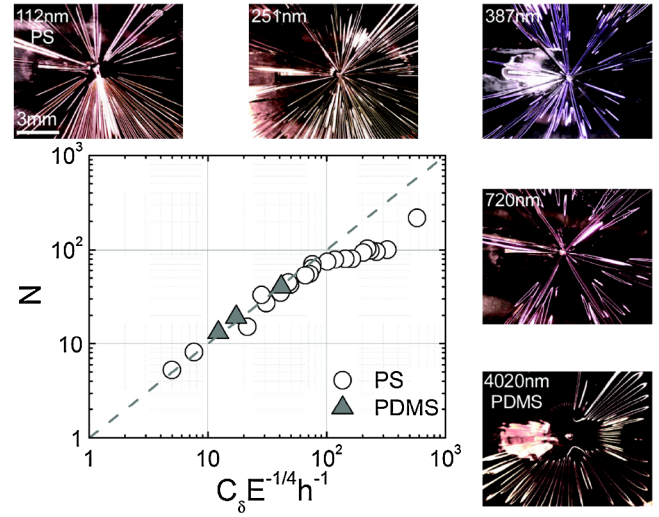

FIG. 2 (color online). A plot of the number of wrinkles, N, versus film thickness, h^{-1}, normalized by material and geometric properties $C_\delta E^{-1/4}$. In our experiments, $C_\delta = 0.005$ Pa$^{1/4}$ m with $a = 0.5$ mm, $\delta = 1$ mm, $L = 17.5$ mm, and $\rho g = 9.8$ kPa/m. Images of wrinkles were obtained by optical microscopy. The dotted line is the predicted scaling of unity from Eq. (2).

displacement, δ_c, is reached as wrinkles collapse into the first fold. The transformation from wrinkle to fold is driven by the increase in wrinkle amplitude with increasing δ, associated with increasing azimuthal compression (Fig. 4). Pocivavsek and Cerda [16] observed a wrinkle-to-fold transition at $\Delta/\lambda \sim 0.3$ for uniaxially compressed films. Since it is more energetically favorable for the film to bend rather than stretch, we can assume that as δ increases the area of the deformed film must be conserved. Therefore, we approximate the azimuthal compression by assuming the shape of the deformed film is an inextensible cone, such
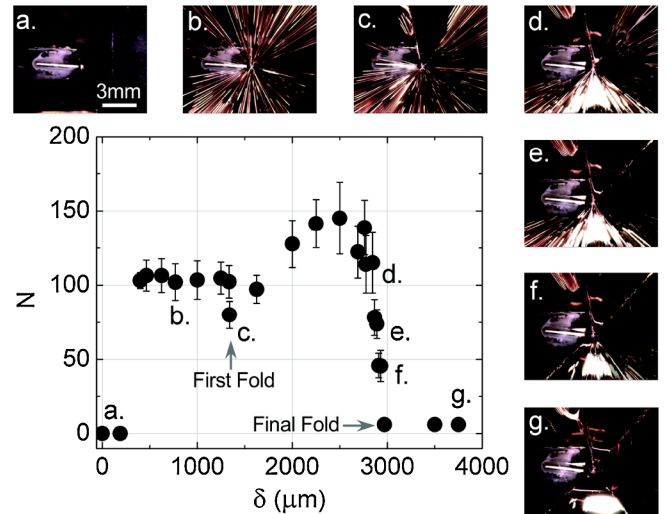

FIG. 3 (color online). Number of wrinkles, N, versus displacement, δ, along with images of wrinkles obtained through optical microscopy for a 91 nm thick polystyrene film.
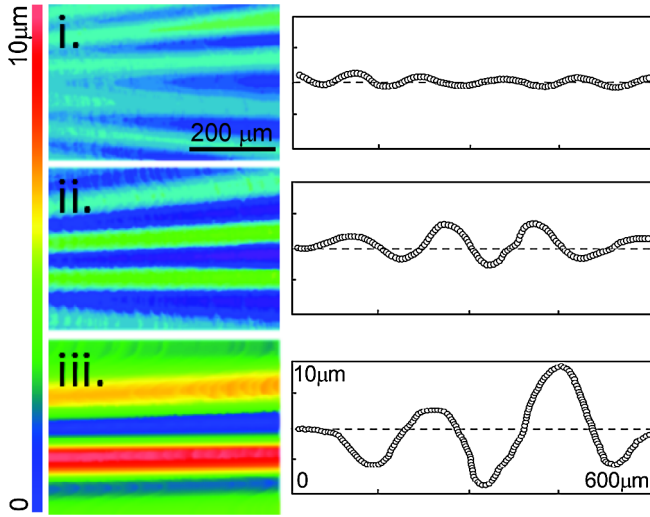
FIG. 4 (color online). Optical profilometry images with corresponding profile plots show the change in wrinkle amplitude. These images show the film with a constant wrinkle wavelength (i), with a growth in wrinkle amplitude (ii), and finally with a further increase in amplitude and decrease in number of wrinkles before folding (iii).

FIG. 5. (a) Force, P, vs displacement, δ, for a 375 nm thick PS film. A fold develops at δ_c at which point the load decreases. Lowering the film causes it to unfold at $\delta_u \approx 0.5$ mm which causes the load to rapidly increase. (b) Hystersis energy of single fold formation, U_{hys}, vs film thickness, h with a linear scaling from Eq. (5). (c) Plot of the critical force and critical displacement for the wrinkle-to-fold transition, P_c and δ_c vs film thickness, h. The dashed line represents a scaling of $h^{4/9}$ from Eq. (3). (d) Radial stress after folding, $\sigma_{rr}^f/\sigma_{rr}^w$ vs film thickness, h with an empirical trend line of h^{-1}.

that $\Delta_\theta = 2\pi L(1 - \sqrt{1 - (\delta/L)^2})$. Using Eq. (2), and the observation of Pocivavsek and Cerda, the critical δ for the wrinkle-to-fold transition should scale as:

$$\delta_c \sim \left(\frac{EL^4}{\rho g}\right)^{1/9} h^{4/9}. \tag{3}$$

This scaling prediction is consistent with our experimental observations [Fig. 5(c)].

The force to deflect the plate can be determined from the deflection of profile of the circular plate at $r = 0$:

$$P = \frac{\pi}{8}\rho g \delta L^2. \tag{4}$$

A representative force versus displacement curve is plotted in Fig. 5(a) [25]. P increases with δ as the film is deformed axisymmetrically until δ_c is reached. Accordingly, $P_c \sim h^{4/9}$ [Fig. 5(c)], based on Eq. (3). At the critical displacement, an instantaneous decrease in P is recorded, and the total energy of the deformed film is minimized through the collapse of several wrinkles into a fold, where strain is localized in a region of maximum curvature [Fig. 3(c)].

Reversing δ to zero, or unloading, after the first fold occurs, demonstrates the development of a hysteretic loop with a change in energy associated with the wrinkle-to-fold transition. [Figure 5(a)]. A representative example of this tendency is given for a 375 nm film in Fig. 5(a) where a fold occurs at a $\delta_c \sim 2$ mm. A large increase in force is measured at $\delta_u \sim 0.5$ mm which corresponds to the film unfolding and returning to its original, planar geometry. The stiffness of the film is always increased upon lowering it back to its original state, leading to a negative intercept for loading. The slope after fold formation will be proportional to the increase in radial tension from folding. The
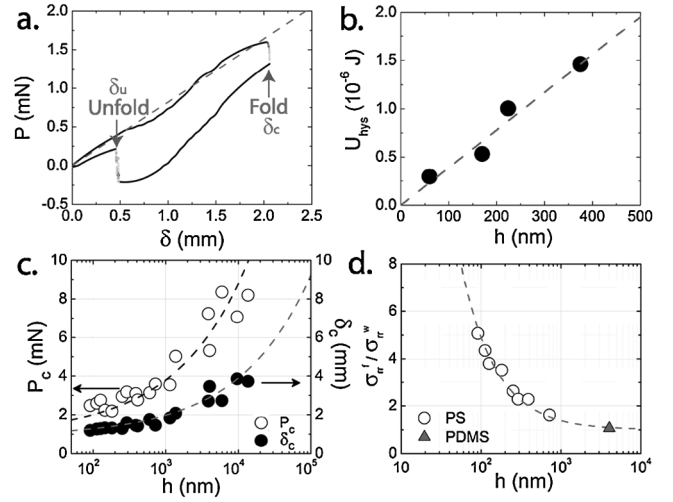
observation of tensile forces at positive displacements is associated with the stretching of the folded ridge, which is formed with minimal length at δ_c. Thus, decreasing δ from δ_c after fold formation requires stretching of the folded ridge. Accordingly, the force after folding is described as $P_f \sim (1 + \omega)P + P_0$, where $\omega \propto \sigma_{rr}^f/\bar{E}$ and σ_{rr}^f is the radial stress after folding [18]. P_0 is the intercept from Fig. 5(a) associated with stretching [18]. The change in energy, U_{hys}, is the difference between the energy for lifting a wrinkled film, $U_w \sim P\delta/2 \sim \rho g \delta^2 L^2$, and the energy for lifting a fold, $U_f \sim \int_{\delta_u}^{\delta_c} P_f d\delta$. Assuming that the folded region is held together by adhesion forces during unloading, the energy U_f will balance the energy to cause adhesive failure, therefore $U_f \sim \gamma L h$, where γ is the surface tension of the film. Using δ_c from Eq. (3), the hysteresis energy becomes

$$U_{\mathrm{hys}} \sim \gamma L h - C_U h^{8/9}, \tag{5}$$

where $C_U \sim (\rho g)^{7/9} L^{26/9} E^{2/9}$. By measuring the hysteresis energy for a variety of film thicknesses we show that U_{hys} scales in a nearly linear manner with film thickness in Fig. 5(b), as predicted by Eq. (5).

The strain localization from the onset of a fold changes the wrinkle wavelength of the remaining wrinkles on the film. Before folding, but after the initial onset of wrinkling, N is weakly dependent on displacement, as predicted by Eq. (2) and shown in Fig. 3. At δ_c, the onset of the wrinkle-to-fold transition, the wrinkle wavelength decreases. This

decrease in the wrinkle wavelength is different from the wrinkle-to-fold transition under uniaxial deformations, where only the wrinkle amplitude decreases upon folding. Under axisymmetric conditions, the wrinkle wavelength decreases, thus implying that the radial stress increases in the surrounding material upon onset of strain localization. According to Eq. (2), $N \sim (\sigma_{rr} a^2 / \bar{E} h^2)^{1/4}$. The presence of the fold will increase the radial stress such that $\sigma_{rr}^f \sim \sigma_{rr}^w (N_f / N)^4$, where N_f is the new number of wrinkles. This increase in stress is inversely dependent on the thickness of the lifted film, as shown in Fig. 5(d), and can lead to stress enhancements as great as a factor of 5. In many ways, this increase in stress is counter intuitive since strain localization is typically associated with energy increase only in the folded region. This increase in the stress in the nonfolded region, demonstrated in Fig. 3, is an important consequence of the axisymmetry. The process of strain localization, which lowers the global energy of a material system, can lead to regions of increased stress beyond the folded region itself. This impact on the surrounding stress field and associated deformation changes (i.e., λ decreases in the nonfolded wrinkles) can impact the development of cells and the general morphology of the morphogenetic field [3].

Further confinement in the film via lifting eventually causes the remaining wrinkles to collapse into folds (Fig. 3). For a fixed probe size, the number of final folds appears independent of film thickness and material properties. A fixed number of folds, 5 ± 1, was observed for both PS and PDMS films across several orders of magnitude of film thickness.

In conclusion, we discussed the wrinkle-to-fold transition observed by lifting an elastic sheet floating on a surface of water. The number of wrinkles is consistent with existing theories at large film thickness (Fig. 2) while the strain energy approximation accurately predicts a load on the film independent of thickness [Eq. (4)]. These experiments create opportunities for further theoretical developments on the impact of folds in various film geometries. Specifically, a more robust understanding of the stress state of the film, the energy associated with unfolding, and the impact of singularities on wrinkle and fold morphologies will help generalize this problem across a variety of systems. Experimentally, it is important to further explore the nonlinear properties of the wrinkle-to-fold transition observed in uniaxial [16] and biaxial loading conditions. Understanding the linear and nonlinear behavior of thin films confined to soft or fluid substrates provides critical insight towards their use in biological and synthetic soft material environments.

*crosby@mail.pse.umass.edu

[1] E. Cerda and L. Mahadevan, Phys. Rev. Lett. **90,** 074302 (2003).
[2] T. A. Witten, Rev. Mod. Phys. **79,** 643 (2007).
[3] J. Bard, *Morphogenesis: The Cellular and Molecular Processes of Developmental Anatomy* (Cambridge University Press, New York, 1990).
[4] W. T. S. Huck, N. Bowden, P. Onck, T. Pardoen, J. W. Hutchinson, and G. M. Whitesides, Langmuir **16,** 3497 (2000).
[5] K. Efimenko, M. Rackaitis, E. Manias, A. Vaziri, L. Mahadevan, and J. Genzer, Nature Mater. **4,** 293 (2005).
[6] E. P. Chan and A. J. Crosby, Soft Matter **2,** 324 (2006).
[7] S. P. Lacour, S. Wagner, Z. Huang, and Z. Suo, Appl. Phys. Lett. **82,** 2404 (2003).
[8] E. Chan, E. Smith, R. Hayward, and A. Crosby, Adv. Mater. **20,** 711 (2008).
[9] A. Boudaoud, E. Hamm, and F. Melo, Phys. Rev. Lett. **99,** 254301 (2007).
[10] E. Cerda, L. Mahadevan, J. M. Pasini, and C. Folds, Proc. Natl. Acad. Sci. U.S.A. **101,** 1806 (2004).
[11] E. Cerda and F. Melo, Nature (London) **401,** 46 (1999).
[12] T. A. Witten, K. Matan, R. B. Williams, and S. R. Nagel, Phys. Rev. Lett. **88,** 076101 (2002).
[13] D. P. Holmes, M. Ursiny, and A. J. Crosby, Soft Matter **4,** 82 (2008).
[14] Y. Forterre, J. M. Skotheim, J. Dumais, and L. Mahadevan, Nature (London) **433,** 421 (2005).
[15] D. P. Holmes and A. J. Crosby, Adv. Mater. **19,** 3589 (2007).
[16] L. Pocivavsek, R. Dellsy, A. Kern, S. Johnson, B. Lin, K. Y. C. Lee, and E. Cerda, Science **320,** 912 (2008).
[17] J. Dervaux and M. Ben Amar, Phys. Rev. Lett. **101,** 068101 (2008).
[18] S. Timoshenko and S. Woinowsky-Kreiger, *Theory of Plates and Shells* (McGraw-Hill, Inc., New York, 1964), 2nd ed.
[19] H. Hertz, Wiedemann's Ann. Phys. Chem (Kyoto) **22,** 449 (1884).
[20] See supplementary material at http://link.aps.org/supplemental/10.1103/PhysRevLett.105.038303 for complete derivation.
[21] J. Huang, M. Juszkiewicz, W. H. deJeu, E. Cerda, T. Emrick, N. Menon, and T. P. Russell, Science **317,** 650 (2007).
[22] E. Cerda, J. Biomech. **38,** 1598 (2005).
[23] J.-C. Géminard, R. Bernal, and F. Melo, Eur. Phys. J. E **15,** 117 (2004).
[24] Deviation from this scaling in the ultrathin film regime may be associated with the nonlinear mechanical properties for ultrathin films or the increasing importance of boundary conditions and constraint at the probe.
[25] Equation (4) indicates that the slope of a P vs δ curve is independent of h and dependent on L. The dashed line corresponds to $L = 20.5$ mm, an error of 17% from our measured radius, $L = 17.5$ mm. This slope is constant for P vs δ data over a large range of h thus confirming the relation.